PROCEEDINGS, Thirty-Seventh Workshop on Geothermal Reservoir Engineering
Stanford University, Stanford, California, January 30 - February 1, 2012
SGP-TR-194

USING MICRO-SEISMICITY AND SEISMIC VELOCITIES TO MAP SUBSURFACE GEOLOGIC AND HYDROLOGIC STRUCTURE WITHIN THE COSO GEOTHERMAL FIELD, CALIFORNIA

J. O. Kaven[1,2], S. H. Hickman[1], and N. C. Davatzes[1]

[1]U.S.G.S. Earthquake Science Center
345 Middlefield Road, MS 977
Menlo Park, CA, 94025, USA
e-mail: okaven@usgs.gov

[2]Temple University
1901 N. 13th St.
Philadelphia, PA 19122

ABSTRACT

We relocate 14 years of seismicity in the Coso Geothermal Field using differential travel times and simultaneously invert for seismic velocities to improve our knowledge of the subsurface geologic and hydrologic structure. We utilize over 60,000 micro-seismic events using waveform cross-correlation to augment the expansive catalog of P- and S-wave differential arrival times recorded at Coso. We further carry out rigorous uncertainty estimation and find that our results are precise to within 10s of meters of relative location error.

Relocated micro-seismicity outlines major, through-going faults in the reservoir in some cases, although a significant portion of seismicity remains diffuse and does not cluster into sharply defined structures. The seismic velocity structure reveals heterogeneous distributions of compressional (V_p) and shear (V_s) wave speed, with V_p generally lower in the main field when compared to the east flank and V_s varying more significantly in the shallow portions of the reservoir. The V_p/V_s ratio appears to outline the two main compartments of the reservoir at depths of approximately 0.5 to 2 km, with a ridge of relatively high V_p/V_s separating the main field from the east flank. In the deeper portion of the reservoir this ridge is less prominent. Our results indicate that high-precision relocations of micro-seismicity and associated velocity inversions can provide useful insights into subsurface structural features and hydrologic compartment boundaries within the Coso Geothermal Field.

INTRODUCTION

Geothermal reservoirs derive their capacity for fluid and heat transport in large part from faults and fractures. Micro-seismicity generated on such faults and fractures can be used to identify larger fault structures as well as fractures that provide access to hot rock and the fluid storage and recharge capacity necessary to have a sustainable geothermal resource. Additionally, inversion for seismic velocities using micro-seismicity permits imaging regions subject to the combined effects of fracture density, fluid/steam content, lithology and other factors.

The Coso Geothermal Field (CGF), located east of the Sierra Nevada batholith, is situated in a tectonically active region that features strike-slip and normal faults as well as numerous magmatic intrusions evident at the surface such as rhyolite domes (Duffield et al., 1980; Manley and Bacon, 2000). Two groups of major faults can be distinguished at the surface based on their orientation and style of faulting (Fig. 1): north-west trending faults with dextral strike-slip that form prominent lineaments with uncertain ages (Duffield et al., 1980; Unruh and Hauksson, 2006; Davatzes and Hickman, 2006) and north to north-east trending normal faults that dip both west and east and may have been active in the Quaternary (Hulen, 1978; Unruh and Hauksson, 2006; Davatzes and Hickman, 2006). These faults appear to divide the reservoir into two distinct compartments: the main field and the east flank (Fig.1).

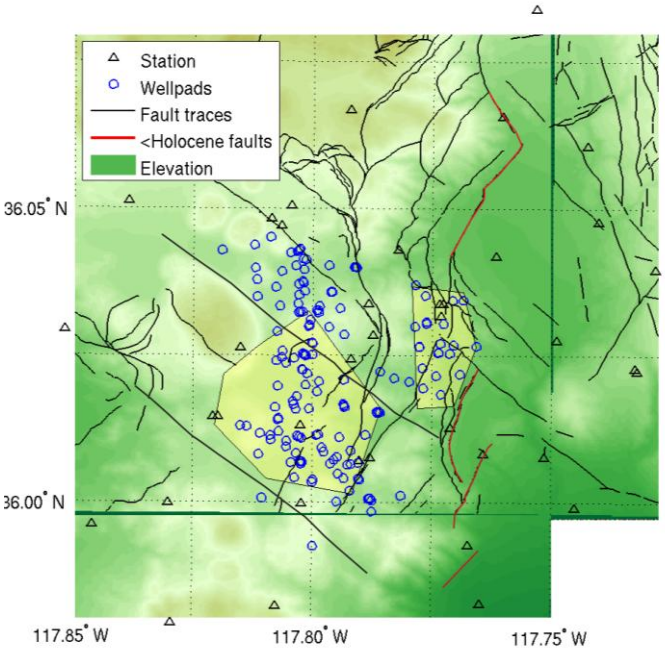

Figure 1: Map of the Coso Geothermal Field (CGF). Yellow shaded polygons indicate the approximate extent of the two main compartments of the CGF: main field and east flank (see Kaven et al. 2011 for details). Wellhead locations are shown as blue circles and the locations of the seismic stations used in thus study are shown as triangles, along with Quaternary fault traces (red where Holocene or younger; see Davatzes and Hickman, 2006, for details).

Seismicity within the CGF occurs both tectonically and as a consequence of injection and production within the field. The seismicity is recorded by the Navy Geothermal Program Office (GPO) using a combination of down-hole and surface seismometers. Initial locations by the GPO generally reveal diffuse clouds of seismicity that occur predominantly in the main field and the east flank. These "clouds" do not clearly coincide with the mapped fault traces at the surface (Fig. 1). (See also Davatzes and Hickman 2006 for a more detailed map). Subsurface imaging of fault structure from reflection seismic (Monastero et al., 2005) or magnetotelluric (MT) imaging (Newman et al., 2008) lacks sufficient resolution; thus, the relationship of these earthquake locations to reservoir-scale fault structure at depth remains poorly constrained.

Several studies have used data recorded by the GPO and surrounding SCSN/USGS networks to analyze earthquakes within and adjacent to the CGF, improve hypocentral locations, and invert for the velocity structure of the greater Coso area (e.g. Lees, 1998; Wu and Lees, 1999; Hauksson and Unruh, 2007; Seher et al., 2011). Others have focused on improving hypocentral locations and obtaining moment tensors for microseismicity associated with individual hydraulic fracturing events (Foulger et al. 2008; Julian et al., 2010). In a regional study of subsurface variations in compressional (V_p) and shear (V_s) velocities from July 1993 to June 1995, Wu and Lees (1999) found low V_p/V_s ratios in the main field at geothermal production depths. They suggest this anomaly might represent a hot, fluid-depleted zone. The goal of our investigation is to better constrain the subsurface geometry of faults that may act as either conduits or barriers to fluid migration and to define the nature and extent of hydrologic compartmentalization within the CGF. We also seek evidence for the relative role of discrete fault zones versus diffuse fracture networks in controlling heat and fluid transport within the reservoir. We build on results from Kaven et al. (2011) with a more extensive analysis of the data to improve locations, develop a newly refined velocity structure, and perform error analyses for relative earthquake locations.

DATA & METHODS

We use seismic data recorded by the Navy GPO from April 1996 to October 2008 at 20 permanent and 30 temporarily deployed stations, most of which are three-component seismometers sampling at either 480Hz or 250Hz. The GPO catalog contains >60,000 earthquakes in the greater Coso region during the time period studied. Consistent measures of hypocentral parameters (location and origin time) and

a reliable, one-dimensional starting velocity model are paramount in any location or velocity structure procedure (Kissling et al., 1994). Our work flow includes the following sequential activities: 1) deriving an initial field-wide, one-dimensional velocity model; 2) inverting for single-event hypocentral parameters using this updated 1D velocity model; 3) inverting for three-dimensional velocity structure using absolute and relative travel times from first arrival data for events with M>0.5; 4) calculating differential travel times for all events in the entire field using first arrival times and waveform cross-correlations together with hypocentral parameters derived in Step 2; and 5) using the three-dimensional velocity structure derived in Step 3 and differential travel times to relocate all events.

We start by relocating all events using a reference 1D velocity model to ensure that consistent measures of hypocentral parameters form the basis of our relocation and velocity inversion efforts. These relocations were performed with a standard Geiger method inversion starting with the reference 1D velocity model of Julian et al. (2008). Long-lasting catalogs are prone to changes in recording, location routines, and velocity model changes that could introduce damaging inconsistencies into hypocentral inversions. We find that origin times of events within the CGF, which are critical for relative relocation, vary significantly between the initial Navy GPO catalog origin times and these 1D locations. These differences range from msec to seconds, with an average difference of 60 msec.

Relocation of seismicity and inversion of the seismic velocity structure is a nonlinear problem and thus strongly dependent on the initial 1D velocity structure (Kissling et al., 1994). We compute the minimum 1D velocity model solution that minimizes travel time residuals during the simultaneous velocity estimation and event location (Kissling et al., 1994). We carry this procedure out for a suite of randomly selected events within the reservoir to establish a consistent and reliable starting model for our subsequent analyses. We invert for velocities over vertical increments of 0.5km and thereby attain a finer vertical resolution than used in the reference model (Julian et al., 2008), which has varying resolution but a 1 km vertical resolution for most segments. We use the updated velocity model to then solve for hypocentral parameters (location and origin time) using standard single-event Geiger method inversions and use these solutions for further analyses.

In actively producing geothermal reservoirs the velocity structure is often highly heterogeneous in three dimensions (Wu and Lees, 1999), which necessitates the use of earthquake location algorithms that allow solving for three-dimensional velocity structure as well. We employ the double-difference earthquake relocation and velocity inversion code tomoDD, which uses a pseudo-bending ray tracing algorithm to find the seismic rays and calculate travel times between events and stations (Zhang and Thurber, 2003). The resulting velocity model is represented as nodes in three dimensions and the velocity values are calculated and linearly interpolated between adjacent nodes. We start with our new 1-D velocity model and derive hypocentral parameters from the single event Geiger method inversions. We then use these hypocentral parameters in our 3D velocity inversion, restricting the analysis to events with M>0.5. We do this for two reasons. First, the computational load is too large when including events at all magnitudes. Second, the largest events generally are recorded on more stations than the smaller ones, providing more ray-paths per event and thus better informing the 3D velocity model. We also tested the heterogeneity of V_p/V_s with coarser grid resolution and find that the general pattern of heterogeneity is reproduced despite the different grid spacing. Finally, at nodes with poor ray path coverage, we do not display the results but retain the initial velocity estimates from the 1D starting model for subsequent relocations.

We then use the 3D velocity model to relocate all seismicity using differential travel times from first arrivals and waveform cross-correlated data without permitting changes in the 3D velocity model. The addition of waveform cross-correlated differential travel times permits higher precision differential travel time measurements and aids in refining the structure within the CGF beyond what is possible with the first arrival data. We apply a causal filter to the waveform data from 5 to 20Hz, the frequency in which most of the energy from these events is contained and across which all seismometers have a constant response. We allow for cross-correlation in 0.5 sec windows around the P-wave arrival and 1 sec around the S-wave arrivals. Differential travel times are used when the correlation coefficient is greater than 0.7, thus ensuring that only very similar waveforms are used. Restricting this analysis to high correlation coefficients also ensures that hypocentral parameters such as location, first motion, and fault attitude, are similar and comparable for correlated events (Waldhauser et al., 2004).

We evaluate relative location errors by means of bootstrapping methods in which input data, i.e. differential travel time estimates, are perturbed by 20 msec, or 5 to 6 times the picking accuracy. These are

standard statistical methods that perturb the data used in the non-linear location procedure to assess the reliability and accuracy of the results (for detailed discussions on the method see Efron, 1982). The perturbation is based on known and estimated errors in picking recorded by the Navy GPO. We find that relative location errors are comparable throughout the central portion of the CGF and are less than 15 m horizontally and less than 30 m vertically; at the margins of the CGF and away from stations these errors increase. The large number of earthquakes requires contiguous patches of seismicity to be relocated that are then merged to form the entire relocated catalog.

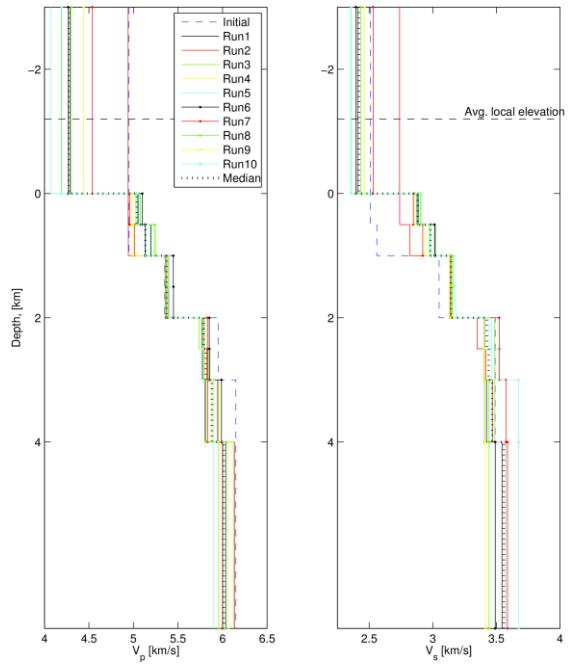

Figure 2: Suite of 1D velocity models based on the initial reference velocity model of Julian et al. (2008). Separate runs correspond to results obtained using randomly selected events throughout the reservoir. The median solution of these runs is used as a starting model for the 3D-velocity inversions and relocations.

RESULTS & DISCUSSION

1D-velocity model

We begin the discussion of our results with the 1D velocity model estimates, since the subsequent analyses (i.e., 3D velocity inversion and relocation) strongly depend on consistent and reliable starting velocity models and hypocentral parameters. We start with the initial (reference) model of Julian et al. (2008) and test for model stability by randomly selecting events with M> 0.5 throughout the reservoir to invert for the field-wide 1D velocity model (V_p and V_s) (Fig. 2). Our inversions indicate slightly different velocities than the initial model (Fig. 2). For example, V_s from our inversion in the shallow portion of the field is higher than the reference model and increases more smoothly with depth. The differences between initial and final models become less significant with greater depth, partly due to fewer events located below 4km, and our velocities ultimately converge on the same velocities as the reference model.

Event locations

We compare the initial locations from the Navy GPO catalog to locations derived using the single-event Geiger method and double difference locations derived using our 3D velocity model from tomoDD (Fig. 3). We restrict ourselves to events with magnitudes M>0.5 in an effort to qualitatively compare the differences between these locations. Improvement in event locations, as interpreted from the definition of discrete structures, is achieved at each step of the relocation process. Event locations located using a standard Geiger method sharpen the catalog when compared to initial Navy GPO catalog locations (compare Figs. 3a and b). The likely reason for the sharpening is the use of a finer, better constrained 1D velocity model and consistent hypocentral parameters. Using the Geiger method derived hypocentral parameters in relative relocations using tomoDD further sharpens the seismicity throughout the entire reservoir (compare Figs. 3b and c). Clusters of relocated events appear to outline linear structures in map-view, in particular in the central portion of the field and within the east flank. Furthermore, clouds of diffuse seismicity become sharper and better distinguish regions of seismicity within both the east flank and the main field.

Maps focusing on smaller subsets of the seismicity (Fig.4) within the east flank using M>0.5 reveal the advantage of relative relocations that utilize differential travel times from waveform cross-correlations in addition to differential travel times derived from first arrivals. In this example, several continuous, co-planar structures become visible and may indicate large-scale faults. Enhanced seismicity in these fault zones likely results from the preferred flow of fluid and accompanying heat; thus, they probably comprise an essential element of this reservoir compartment. Relocation of the entire catalog of M>0.5 events in the CGF utilizing differential travel times from first arrivals and waveform cross correlations is nearing completion.

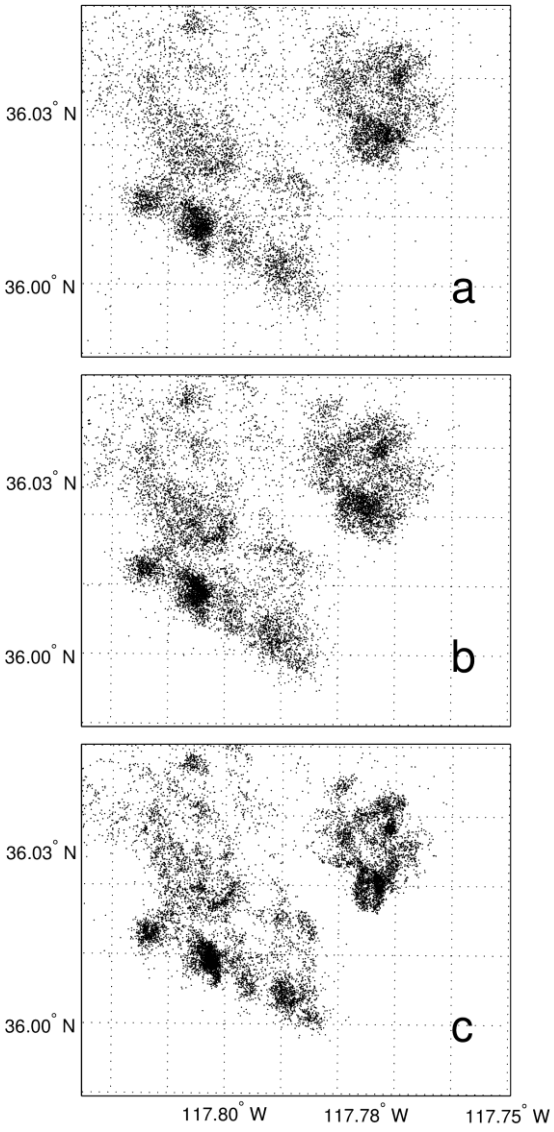

Figure 3: Comparison of event locations throughout the reservoir: a) Navy-GPO catalog; b) Geiger method single-event locations using refined 1D-velocity model; c) relative relocations using differential travel times. Only events with $M \geq 0.5$ are depicted here to highlight the sharpening of seismicity clouds. Note the emergence of sharp boundaries of seismicity, in particular in the east flank and the southwestern edge of the main field.

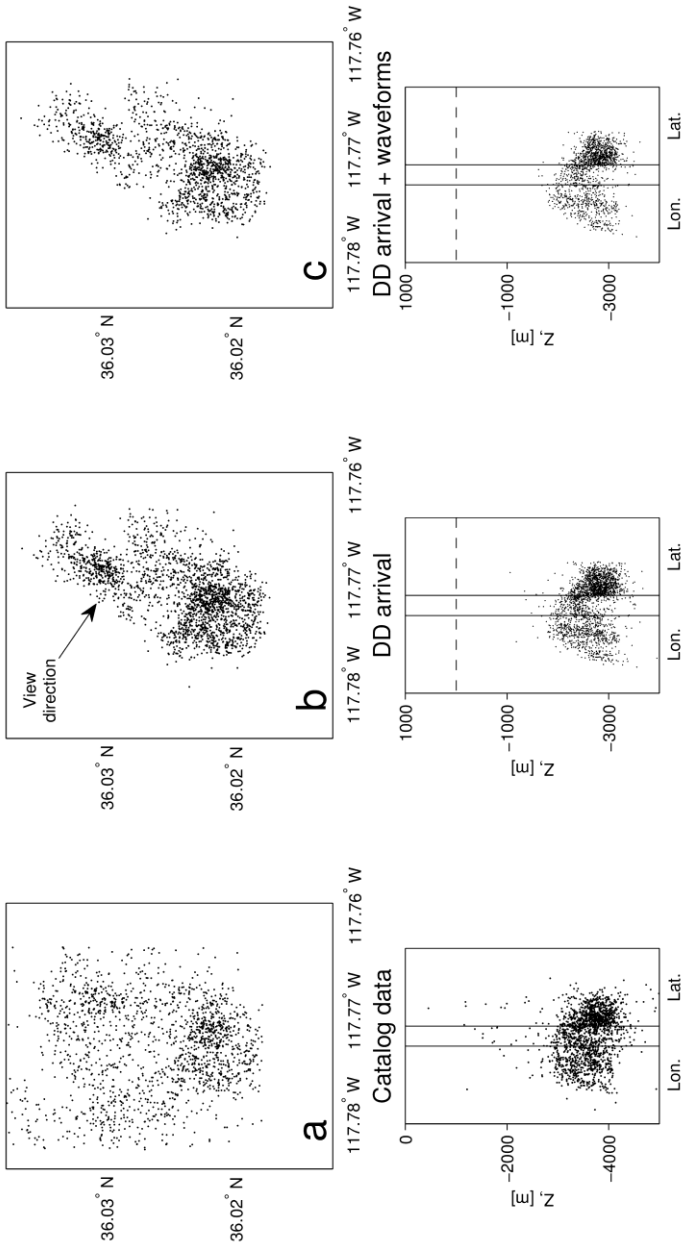

Figure 4: Subset of the East flank seismicity (southeastern portion, $M \geq 0.5$) in map and cross-section view. View direction indicated on map view. a) Navy GPO catalog data; b) relocated data using differential travel times (double difference, or DD) derived from arrival times only; c) relocated data using differential travel times derived from arrival times (DD) and waveform cross-correlation.

3D velocity models

The seismic velocity structure obtained from our inversion of the relocated seismicity reveals heterogeneous distributions of V_p and V_s along horizontal slices through the field (Fig.5). In the shallow portion of the CGF (d = 0 km, with all depths discussed herein relative to mean sea level), V_p is higher in both the main field and in the northern portion of the east flank as compared to adjacent portions of the field. At greater depths (d = 1.5 to 3 km), high V_p is evident only in portions of the main field and north of it; V_p is lower in the deep east flank (d = 3 km) than the surrounding area.

V_s exhibits relative highs near the east flank and in the main field at shallow to intermediate depths (d = 0 to 1.5 km). Julian et al. (2008) suggest that regions of high V_s within the shallow main field may reflect decreases in fluid pressure relative to adjacent portions of the field. This is consistent with our observation of relatively high V_s within the main field at depths of 0 to 1.5 km, which coincides with seismicity associated with ongoing geothermal production. In contrast, the relatively low V_s in the deeper portion of the east flank may indicate elevated fluid or steam pressures. However, in making these comparisons, it should be noted that it is difficult to differentiate between the effects of fluid saturation versus fluid pressure on V_p or V_s, so these variations could also reflect differences in fluid saturation state.

The ratio of shear to compressional wave speeds (V_p/V_s ratio) is commonly used to infer sub-surface variations in rock and fluid properties, with V_p/V_s being most sensitive to changes in temperature, effective stress (normal stress minus pore pressure), porosity/pore geometry (including fractures), and fluid saturation state (e.g., Wu and Lees, 1999). In low porosity crystalline rock, such as the granitic rocks comprising the CGF, decreases in V_p/V_s ratio are generally attributed to increases in temperature or decreases in porosity, water saturation or fluid pressure (O'Connell and Budiansky, 1974; Chatterjee et al., 1985). Regions of low Vp/Vs can be found at all depths within the CGF (Fig. 6) and the distribution is highly heterogeneous.

Both the east flank and the main field reveal heterogeneous distributions of V_p/V_s, which coincide with the densest clusters of seismicity (c.f. Fig. 3). Seismicity associated with geothermal production is present in both portions of the CGF at depths of 1 to 1.5 km (Figs. 3 and 4) and thus we postulate that these localized decreases in V_p/V_s are most likely due to relatively low water saturation or fluid pressure due to ongoing geothermal production or may result from naturally elevated temperatures within the main field and east flank. While the main field and east flank experience generally reduced V_p/V_s at intermediate depths as compared to surrounding areas, the heterogeneity within them likely indicates the presence of sub-compartments. Also note the increased V_p/V_s between the east flank and main field at intermediate depths (1 to 1.5 km). This region of high V_p/V_s appears to separate these compartments and is also devoid of seismicity with $M \geq 0.5$ (Fig. 3). Furthermore, the heterogeneous distribution of V_p/V_s outside of these main compartments may indicate that the reservoir has several major and minor compartments in which seismic velocities and their ratio can differ significantly.

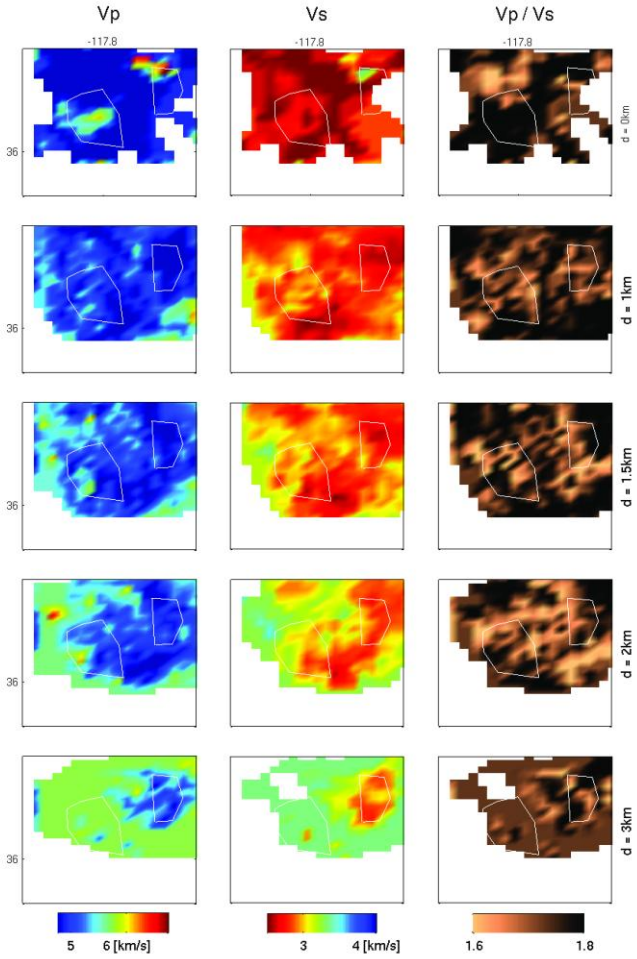

Figure 5: Inverted seismic velocities: V_p (left column), V_s (middle column), and V_p/V_s (right column) with increasing depth relative to sea-level, d. White polygons highlight the approximate extents of the main field and east flank compartment (c.f. Fig. 1). Results are only displayed when sufficient ray-path coverage exist near inversion nodes.

CONCLUSIONS

The results of our analyses underscore that double-difference relative relocation techniques provide a powerful tool to identify finer structure within geothermal systems. These fault zones and fracture networks are likely to be the major pathways for heat and fluid flow in crystalline, low porosity systems such as the Coso Geothermal Field. Our results indicate that major structural features may be elucidated by our event relocations, with work on-going to verify these findings.

Our analysis shows that consistent measures of hypocentral parameters and a reliable starting velocity model are indispensable ingredients in generating reliable earthquake relocations and velocity inversions, without which even single-event locations can produce flawed results. We further establish that relative location errors can be reduced to less than 15 m horizontally (and 30 m vertically) using this approach. Our current results indicate vast improvements in sharpening of clouds of seismicity as well as reduction in relative errors over prior attempts that relied solely on initial travel times (Kaven et al., 2011).

These results reveal a sharpened image of the CGF that includes major, and possibly minor, structures that host concentrations of seismicity not evident in the un-processed catalog alone. A large portion of the seismicity, however, remains diffuse away from major structural features. This suggests that seismicity generated throughout the reservoir on small-scale features, i.e. small-displacement faults and fractures, plays an important role in providing and maintaining the permeability needed for viable energy production within the CGF. The two main compartments, the main field and east flank, are separated by a region largely devoid of seismicity. Heterogeneous distributions of seismic velocities and velocity ratios suggest that finer-scale compartmentalization may take place within the main field, east flank and perhaps other portions of the Coso Geothermal Field.

REFERENCES

Chatterjee, S.N., Pitt, A.M., and Iyer, H.M. (1985), "Vp/Vs ratios in the Yellowstone National Park Region, Wyoming" *Journal of Volcanology and Geothermal Research*, **26**, 213-230.

Davatzes, N. C. and Hickman, S. H.. (2006), "Stress and faulting in the Coso geothermal field: update and recent results from the East Flank and Coso Wash" *Proceedings 31st Workshop on geothermal Reservoir Engineering, Stanford University, Stanford, California, January 30 – February 1. 2006,* SGP-TR-179, 12p.

Duffield, W. A., Bacon, C. R., and Dalrymple, G. B. (1980), "Late Cenozoic volcanism, geochronology and structure of the Coso Range, Inyo County, California" *Journal of Geophysical Research*, **85**, 2381-2404.

Efron, B. (1982), "The Jackknife, the Bootstrap, and Other Resampling Plans", *SIAM*, 92 p.

Evans, J.R., Eberhart-Phillips, D. and Thurber, C.H. (1994), "User's manual for SIMULPS12 for imaging Vp and Vp/Vs: a derivative of the "Thurber" tomographic inversion SIMUL3 for local earthquakes and explosions" *U.S.Geological Survey, Open File Report*, 94-431, 100pp.

Foulger, G.R., Julian, B.R. and Monastero, F. C. (2008), "Seismic monitoring of EGS tests at the Coso Geothermal area, California, using accurate MEQ locations and full moment tensors" *Proceedings 33rd Workshop on geothermal Reservoir Engineering, Stanford University, Stanford, California, January 28 – 30, 2008,* SGP-TR-179, 8p.

Hauksson, E. and Unruh, J. (2007), "Regional tectonics of the Coso geothermal area along the intracontinental plate boundary in central eastern California: Three-dimensional Vp and Vp/Vs models, spatio-temporal seismicity patterns, and seismogenic deformation" *Journal of Geophysical Research*, **112**, B06309.

Hulen, J. B. (1978), "Geology and alteration of the Coso geothermal area, Inyo County, California" *U.S. Dept. of Energy: Geothermal Energy*.

Julian, B.R., Foulger, G.R. and Monastero, F. C. (2008), "Time-dependent seismic tomography and its application to the Coso Geothermal Area, 1996-2006" *Proceedings 33rd Workshop on geothermal Reservoir Engineering, Stanford University, Stanford, California, January 28 – 30, 2008,* SGP-TR-185, 4p.

Julian, B.R., G.R. Foulger, F.C. Monastero and S. Bjornstad (2010), "Imaging Hydraulic Fractures in a Geothermal Reservoir", *Geophys. Res. Lett.*, **37**, L07305, 10.1029/2009GL040933

Kaven, J.O., Hickman, S.H. and Davatzes, N.C. (2011),"Micro-Seismicity, Fault Structure, and Hydrologic Compartmentalization Within the Coso Geothermal Field, California", *Proceedings 36rd Workshop on geothermal Reservoir Engineering, Stanford University, Stanford, California, January 31 – February 2, 2011,* SGP-TR-191, 8p.

Kissling, E., Ellsworth, W.L., Eberhart-Phillips, D. and Kradolfer, U. (1994), “Initial reference models in local earthquake tomography”, *Journal of Geophysical Research*, **99**, no. B10, 19635-19646

Lees, J. M. (1998), "Multiplet Analyses at Coso Geothermal” *Bulletin of the Seism. Soc. America*, **88**, no.5, 1127-1143.

Manley, C.R. and Bacon, C.R. (2000), “Rhyolite thermobarometry and the shallowing of the magma reservoir, Coso volcanic field, California”, Journal of Petrology, **41**, p. 149-174.

Monastero, F.C., Katzenstein, A.M., Miller, S.J., Unruh, J.R., Adams, M.C. and Richards-Dinger, K. (2005), “The Coso geothermal field: A nascent metamorphic core complex”. *GSA Bull.*, **177**(11/12), 1534-1553.

Newman, G.A., Gasperikova, E., Hoversten, G.M., and Wannamaker, P.E. (2008), “Three-dimensional magnetotelluric characterization of the Coso geothermal field”, *Geothermics*, **37**, p. 369-399.

O'Connell, R.J., and Budiansky, B. (1974), "Seismic velocities in dry and saturated cracked solids” *Journal of Geophysical Research*, **79**, no. 35 5412-5426.

Schaff, D.P., Bokelmann, G.H.R., Beroza, G.C., Waldhauser, F., and Ellsworth, W.L. (2002) “High resolution image of the Calaveras Fault seismicity” *Journal of Geophysical Research*, **107**, no.B9, 2186, doi 10.1029/2001JB000633.

Schaff, D.P., Bokelmann, G.H.R., Ellsworth, W.L., Zanzerkia, E., Waldhauser, F., and Beroza, G.C. (2004), "Optimizing correlation techniques for improved earthquake location” *Bulletin of the Seism. Soc. America*, **94**, no.2, 705-7021.

Seher, T., Zhang, H. Fehler, M., Yu, H., Soukhovitskaya, V., Commer, M. and Newman, G. (2011), “Temporal Velocity Variation beneath the Coso Geothermal Field Observed using Seismic Double Difference Tomography of Compressional and Shear Wave Arrival Times”, *GRC Transactions*, **90**, p. 1743-1747.

Unruh, J. and Hauksson, E. (2006), “Active faulting in the Coso Geothermal Field, eastern Califnorina”, Geothermal Resources Council Transactions, **30**, p. 165-170.

Waldhauser, F. and Ellsworth, W.L. (2000), “A double-difference earthquake location algorithm: method and application to the northern Hayward Fault, California”, *Bulletin of the Seism. Soc. America*, **90**, 1353-1368.

Waldhauser, F., Ellsworth, W.L., Schaff, D.P. and Cole, A. (2004), “Streaks, mulitplets, and holes: High-resolution spatio-temporal behavior of Parkfield seismicity”, Geophysical Research Letters, 31, doi:10.1029/2004GL020648.

Wu, E. and Lees, J. M. (1999), "Three-dimensional P and S wave velocity structures of the Coso Geothermal Area, California, from microseismic travel time” *Journal of Geophysical Research*, **104**, no. B6, 13217-13233.

Zhang, H. and Thurber, C.H. (2003), “Double-Difference tomography: the method and its application to the Hayward Fault, California”, *Bulletin of the Seism. Soc. America*, **93**, no.5, 1875-1889.